Effect of Ambient Atmosphere and Temperature on The Corrosion Resistance of X80 High-deformation Pipeline Steel in Bicarbonate Solution

Wei Zhao[1,*], Hui Zhang[1], Yong Zou[2]

[1] School of mechanical & automotive engineering, Qilu University of Technology, Jinan 250353, China
[2] Key Laboratory for Liquid-Solid Structural Evolution & Processing of Materials Ministry of Education, Shandong University, Jinan 250061, China
[*]E-mail: zwapple@yeah.net

In this study, the electrochemical corrosion behavior of X80 high-deformation pipeline steel in bicarbonate solutions was evaluated. Effects of atmosphere and temperature on the corrosion resistance were studied by electrochemical tests. Results showed that the main characteristics of the potentiodynamic polarization curves are mainly determined by the atmosphere. The solution concentration and temperature can only affect the specific values. The presence of O_2 can accelerate the corrosion reactions, resulting in "double-anodic-peak-phenomenon". CO_2 weakens the stability of passivity, even eliminates the passivity phenomenon in dilute solution. Results of the potentiodynamic polarization, electrochemical impedance spectroscopy, potentiostatic anodic polarization, and Mott–Schottky analysis indicated that the corrosion rate increases and the passivity stability weakens, with the increase in temperature.

1. INTRODUCTION

Demands for oil, gas, and other energy sources have been increasing with the development of global economy. As pipeline transportation is the vital way to deliver these energy sources, high-strength, low-alloyed (HSLA) pipeline steels have been used widely to reduce pipeline investment and increase delivery speed [1, 2]. As a result, increasing attention has been focused on research related with HSLA in recent years [3]. On the other hand, pipeline has to traverse a large number of

earthquake-prone regions, perennial cryolithic zones and other dangerous regions so that pipeline steels with high sustain deformation ability have been paid much attention. X80 high deformation (X80HD) pipeline steel has high strength level, the same as X80, and high resistance of deformation, which has high potential to be used widely in the world.

Corrosion of pipeline steels, which depends on the internal and external environments of pipelines, is difficult to predict and control [4-7]. Almost 60% of oil pipeline corrosion failures in the USA are attributed to an inadequate understanding of the corrosive capabilities of dissolved species [8]. Corrosion contributes to the danger of pipeline and huge cost [9]. Although numerous studies have been conducted on the corrosion resistance of pipeline steel in alkaline [10-12], near-neutral [3, 13-17], and acid environments [12, 18-25] with or without applied stress [3, 10, 26-28], the corrosion mechanism remains unclear. In addition, X80HD pipeline steel is very different from traditional X80 pipeline steel, in the aspect of microstructure and properties. Thus, it is necessary to study the corrosion resistance of X80HD pipeline steel.

As is shown in Ref. [4, 8, 29], the pipeline flows may encounter a mildly-alkaline corrosion environment, especially after excessive inhibitor injection, in which bicarbonate exists with high concentrations and acts as a major agent in the dissolution of pipeline steels. And actually in the near-neutral and high pH solutions, bicarbonate plays an important factor in the anodic and cathodic reactions at internal and external of pipeline [8, 30, 31]. It is necessary to study the corrosion resistance of X80HD pipeline steels in the bicarbonate solutions. In this study, conventional potentiodynamic polarization, electrochemical impedance spectroscopy (EIS), potentiostatic anodic polarization, and Mott–Schottky analysis were used to study effects of atmosphere, solution concentration, and temperature on the corrosion of X80HD pipeline steel in bicarbonate solution. CO_2 corrosion is also a very serious problem in oil and gas industry, which can easily cause the failure of pipelines and result in great accidents [32]. In this study, effects of CO_2 on the corrosion resistance of X80HD pipeline steels in bicarbonate solutions were also studied.

2. EXPERIMENTAL METHODS

2.1. Test materials

X80HD steel was produced by thermo-mechanically controlled processing. The dimensions of the steel samples were 10 mm×10 mm. The composition of X80HD, used in this study, is (wt.%): C 0.046, Si 0.305, Mn 1.76, P 0.007, S 0.001, Al 0.058, Nb 0.079, V 0.008, Ni 0.225, Cr 0.023, Mo 0.226, B 0.00025, Ti 0.015, Ca 0.001, Cu 0.215 and Fe balance. The microstructure features examined with the use of optical microscopy are shown in Fig. 1. The steel mainly consists of polygonal ferrite (mild phase) and granular bainite (hard phase). Mild phase and hard phase distribute uniformly.

Prior to electrochemical tests, the samples were ground up to 800 grit silicon, then soldered to copper wires, mounted in silica gel, rinsed with deionized water, degreased in acetone, cleaned ultrasonically with ethyl alcohol for 15 min and then air dried.
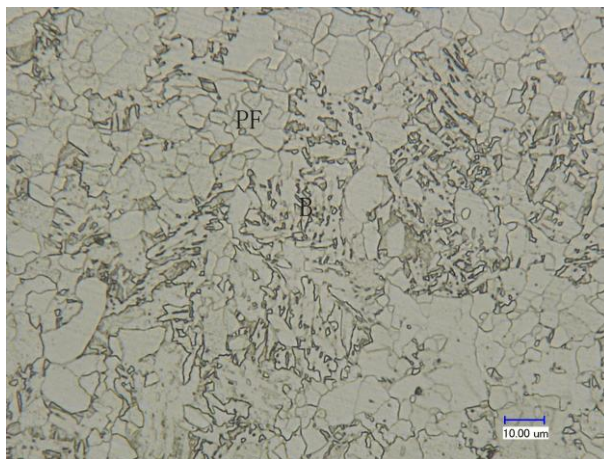
Figure 1. Optical microscope of the Microstructure of X80HD pipeline steel

2.2. Test solution

The test solutions were obtained by adding 0.1, 0.5, and 0.9 M (mol·L^{-1}) NaHCO$_3$ in deionized. Three atmosphere environments were prepared. The first environment was aerated without gas flux ("aerated"). In the second environment, the solutions were first purged for 60 min with continuous Ar for deoxygenation and the purging was maintained during the entire electrochemical tests ("with continuous Ar"). In the third condition, CO$_2$ was employed instead of Ar ("with continuous CO$_2$"). To evaluate the effects of temperature on corrosion resistance, the solution concentration was fixed at 0.5 M, the atmosphere condition was aerated, and the temperature values employed were 25, 40, 60, and 80 °C, maintained within ±1°C.

2.3. Electrochemical tests

A three-electrode electrochemical cell system was employed with the use of the studied material, X80HD pipeline steel, as the working electrode, platinum plate as the counter electrode, and saturated calomel electrode (SCE) of +0.241 V_{SHE} as the reference electrode. After immersing the samples in solutions, a potentiostatic -1.2 V vs. SCE catholic conditioning for 5 min was performed to dissolve air-formed oxides. The electrochemical experiments were then conducted. The EIS tests were performed at the open circuit potentials (OCP) to study the electrochemical interactions at the stable OCP conditions from 0.01 Hz to 100 kHz. Potentiodynamic polarization scans were obtained at 1 mV/s sweep rate from -1.2 V vs. SCE to 1.2 V vs.SCE. After potentiodynamic polarization tests, the corrosion morphologies were observed. To evaluate the characteristics of the formed passive film, the potentiostatic polarization tests were performed at 0.5 V vs. SCE for 3600 s at different temperatures, and then the Mott–Schottky tests were performed at a potential scan from -0.6 V vs. SCE to 0.9 V vs. SCE at 1000 Hz. Each test was repeated at least three times to ensure the reproducibility of the results.

Mott–Schottky relationship expresses the potential dependence of the capacitance of space-charge layer (*C*):

$$\frac{1}{C^2} = \frac{2}{e\varepsilon\varepsilon_0 N_d A^2}(E - \phi_{fb} - \frac{kT}{e}) \qquad \text{for n-type semiconductor} \qquad (1)$$
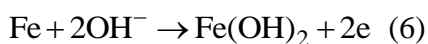
$$\frac{1}{C^2} = \frac{2}{e\varepsilon\varepsilon_0 N_a A^2}(E - \phi_{fb} - \frac{kT}{e}) \qquad \text{for p-type semiconductor} \qquad (2)$$

where e is electron charge (1.60×10^{-19} C), ε is dielectric constant of iron oxide (15.6) [33], ε_0 is the vacuum permittivity (8.85×10^{-14} F·cm^{-1}), E is the applied potential (the horizontal ordinate in the Mott–Schottky plots), k is Boltzmann constant (1.38×10^{-23} J·K^{-1}), T is absolute temperature ($t + 273.15$K), and A is the area of the specimen, taken as 1 cm^2 in the experiments. N_d and N_a are the donor and acceptor density, respectively, which can be determined from the slope of the linear relationship (K) in the Mott–Schottky plots.
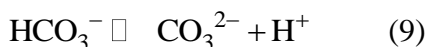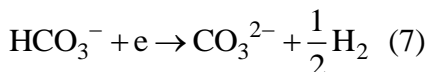
3. RESULTS AND DISCUSSION

3.1. Effects of atmosphere

The potentiodynamic curves of X80HD pipeline steel in different NaHCO$_3$ solutions under various atmosphere environments are shown in Fig. 2. The specific fitting values are listed in Table 1. The figures showed that the main characteristics of potentiodynamic polarization curves are determined by atmosphere, and the solution concentration can only affect the specific values. In the three atmospheric conditions, the corrosion potential (E_{corr}) and Tafel slopes (b_a and b_c) decreases, but the corrosion current density (i_{corr}) and the corrosion rate (v) significantly increase with the increase in solution concentration which can be attributed to its accelerating effects on anodic and cathodic reactions [8]. Except for the sample in 0.1 M solution with continuous CO$_2$, the passivity phenomenon is observed in all other conditions. The passivation potential (E_{pass}) is approximately -0.6 V vs. SCE and the passivity is produced by corrosion products of FeCO$_3$ and Fe(OH)$_2$, as follows [1, 34-39]:

$$Fe + HCO_3^- \rightarrow FeCO_3 + H^+ + 2e \qquad (3)$$

$$Fe + CO_3^{2-} \rightarrow FeCO_3 + 2e \qquad (4)$$

$$Fe(OH)_2 + HCO_3^- \rightarrow FeCO_3 + H_2O + OH^- \qquad (5)$$

$$Fe + 2OH^- \rightarrow Fe(OH)_2 + 2e \qquad (6)$$

where CO$_3^{2-}$ is generated by cathodic reactions and the ionization of HCO$_3^-$ [8], as follows:

$$HCO_3^- + e \rightarrow CO_3^{2-} + \frac{1}{2}H_2 \qquad (7)$$

$$HCO_3^- + e \rightarrow CO_3^{2-} + H_{ads} \qquad (8)$$

$$HCO_3^- \square \; CO_3^{2-} + H^+ \qquad (9)$$
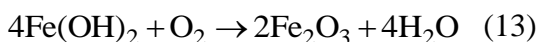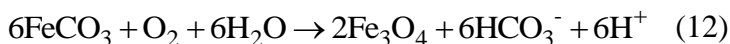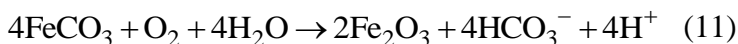
The transpassivation potential ($E_{tranpass}$) is approximately 0.9 V vs. SCE, which are independent of the solution concentration and atmosphere (except for the 0.1 M solution with continuous CO$_2$). There's no obvious connection between the transpassivation and atmosphere which is different from the results of reference [8].The separate investigations on the electrochemical of bicarbonate at high potentials should be carried out to find the fundamental reasons.

The current densities in the passive region are maintained $10^{-4.8} A \cdot cm^{-2}$ in the aerated solutions, indicating that the stability of passivation is almost independent of the solution concentration. Moreover, the second anodic peak is observed at -0.3 V vs. SCE. The increase of current density may be attributed to the dissolution of $Fe(OH)_2$ in HCO_3^- as follows [29]:

$$4Fe(OH)_2 + HCO_3^- \rightarrow CO_3^{2-} + OH^- + Fe^{2+} + H_2O \quad (10)$$
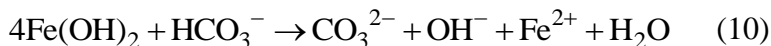
In addition, the further decrease of current density may be caused by the further oxidation of $FeCO_3$ and $Fe(OH)_2$ to Fe_2O_3 and Fe_3O_4 by O_2 [1, 34]:

$$4FeCO_3 + O_2 + 4H_2O \rightarrow 2Fe_2O_3 + 4HCO_3^- + 4H^+ \quad (11)$$

$$6FeCO_3 + O_2 + 6H_2O \rightarrow 2Fe_3O_4 + 6HCO_3^- + 6H^+ \quad (12)$$
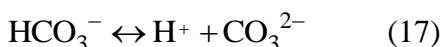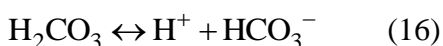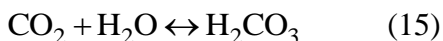
$$4Fe(OH)_2 + O_2 \rightarrow 2Fe_2O_3 + 4H_2O \quad (13)$$

The presence of "double anodic peak phenomenon" can be attributed to the presence of O_2. It is absent in solutions with continuous Ar or CO_2 which can be attributed to the vast majority of HCO_3^- participating in the cathodic reactions.

The anodic and cathodic Tafel slopes and corrosion rate in solutions with continuous Ar is much smaller than that in aerated conditions. This observation demonstrates that the presence of O_2 can promote anodic and cathodic corrosion reactions. The cathodic reactions involve dissolved O_2 [34]:

$$O_2 + 2H_2O + 4e \rightarrow 4OH^- \quad (14)$$
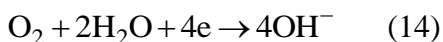
At this moment, the passive range is almost the same as that in aerated conditions, demonstrating that the passivation of X80HD is mainly due to the presence of HCO_3^-, and the presence of O_2 only aids in stabilizing the passivity. Under continuous Ar, i_{pass} becomes more negative and exhibits stable passivity with the increase in solution concentration.

Under continuous CO_2, the following reactions occurred [38, 39]:

$$CO_2 + H_2O \leftrightarrow H_2CO_3 \quad (15)$$

$$H_2CO_3 \leftrightarrow H^+ + HCO_3^- \quad (16)$$

$$HCO_3^- \leftrightarrow H^+ + CO_3^{2-} \quad (17)$$

Previous studies [4] showed that H_2CO_3 plays an important role in accelerating the corrosion reactions in bicarbonate solutions indicating the higher corrosion rate in solutions with continuous CO_2. Although bicarbonate preserved its cathodic and anodic influences, CO_2 remarkably accelerates the reactions, resulting in the decrease of Tafel slopes and twofold increase of corrosion rate compared with those in aerated condition or with continuous Ar. According to Ref.[40], H_2CO_3 exists with comparable concentrations of approximately 1.8×10^{-5} mol·kg^{-1} in the three solutions, but the ionization degrees of H_2CO_3 vary. In dilute solutions, the ionization degree of H_2CO_3 and H^+ concentration are relatively high because of the low pH so that no passivity is observed in the 0.1 M solution. In 0.5 and 0.9 M solutions, although passivity exists, the i_{pass} is much more than that in aerated condition and with continuous Ar, resulting in unstable passive film. In addition, looser corrosion products and some pitting holes can be introduced in the CO_2 environments even without Cl$^-$ [41], which is one of the reasons for the disappearance or instability of the passivity.
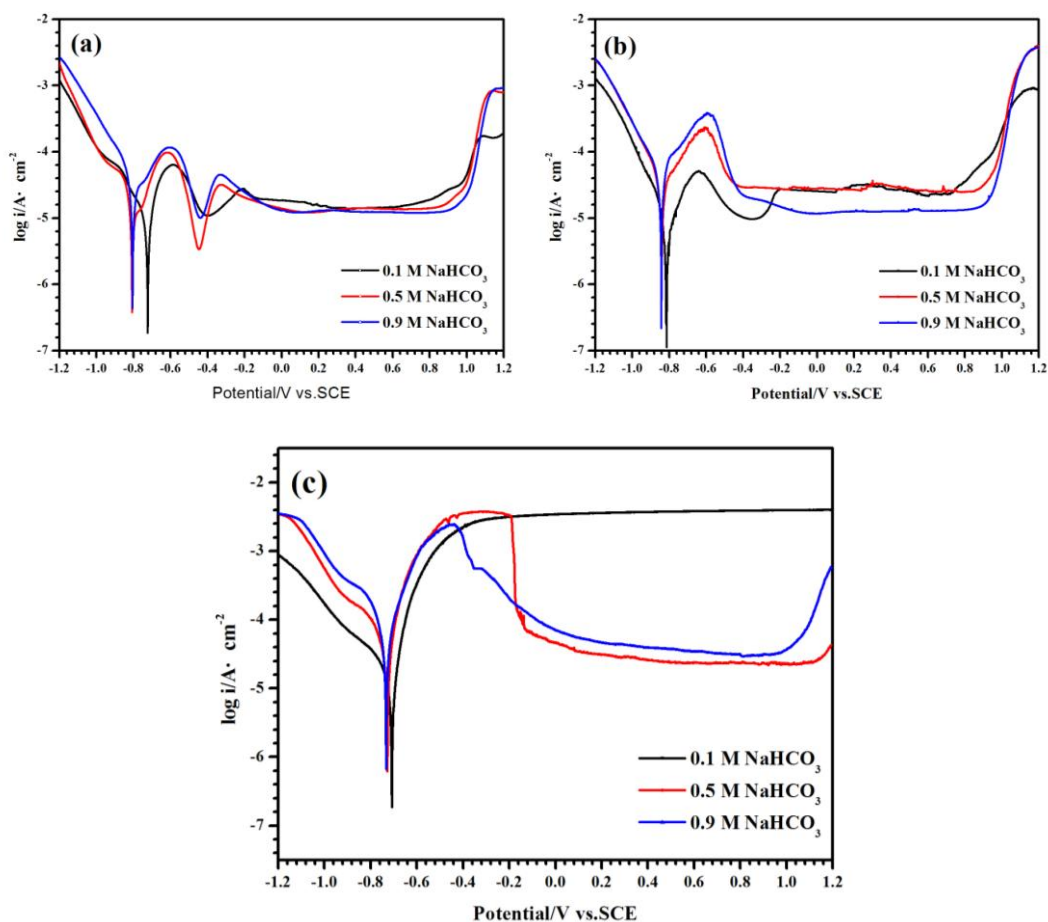
Figure 2. The potentiodynamic polarization curves of X80HD pipeline steel in 0.1, 0.5 and 0.9 M NaHCO$_3$ solution when aerated, with continuous Ar or CO$_2$ gas: (a) aerated; (b) with continuous Ar and (c) with continuous CO$_2$

Table 1. Corrosion parameters of potentiodynamic polarization profiles in each case (in which M means mol·L^{-1})

Atmosphere	c/M	0.1	0.5	0.9
Aerated	b_a/V·dec^{-1}	5.48	5.18	3.96
	b_c/V·dec^{-1}	-5.56	-4.65	-3.89
	E_{corr}/V vs. SCE	-0.722	-0.807	-0.808
	i_{corr}/μA·cm^{-2}	3.37	16.76	37.47
	v/mm·a^{-1}	0.078	0.143	0.871
With continuous Ar	b_a/V·dec^{-1}	6.94	6.05	5.45
	b_c/V·dec^{-1}	-7.15	-5.65	-5.05
	E_{corr}/V vs. SCE	-0.813	-0.820	-0.842
	i_{corr}/μA·cm^{-2}	2.62	11.14	18.72
	v/mm·a^{-1}	0.244	0.259	0.435
With continuous CO$_2$	b_a/V·dec^{-1}	4.65	3.21	2.75
	b_c/V·dec^{-1}	-3.20	-2.74	-2.29
	E_{corr}/V vs. SCE	-0.707	-0.728	-0.733
	i_{corr}/μA·cm^{-2}	5.87	63.79	76.14
	v/mm·a^{-1}	0.136	1.483	1.770

3.2 Effects of temperature
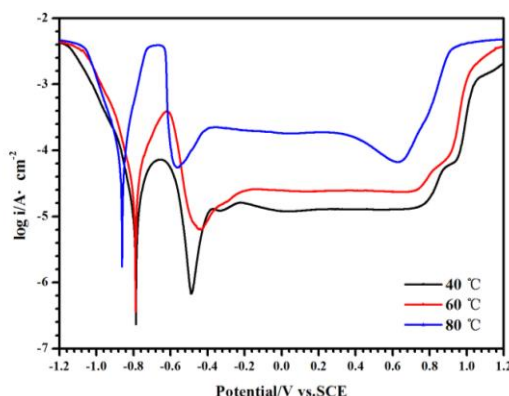
3.2.1 Potentiodynamic polarization tests

The potentiodynamic polarization curves of X80HD pipeline steel in 0.5 M NaHCO$_3$ aerated solutions at 40, 60, and 80 °C are shown in Fig. 3. Fitting results are shown in Table 2. Figs. 1 and 5 illustrate that the changes in temperature do not affect the main characteristics of the potentiodynamic polarization curves, only the quantitative values. With the increase in temperature from 25 °C to 80 °C, anodic and cathodic Tafel slopes and corrosion rate considerably increase. This is in accordance with the previous studies [4, 8].

The following equations were obtained through least-square methods:

$i_{corr} = 1.025t$-8.265 (18)

$v = 0.01156t$-0.0605 (19)

The two formulas show that i_{corr} and v increase linearly with increasing temperature. Thus, temperature significantly affects the corrosion resistance of X80HD in NaHCO$_3$ solution.


Figure 3. Effects of temperatures (40, 60 and 80 ℃) on potentiodynamic polarization curves of X80HD pipeline steel in 0.5 M NaHCO$_3$ aerated solution

Table 2. Corrosion parameters of potentiodynamic polarization curves in different temperatures

| t/°C	E_{corr}/V vs. SCE	i_{corr}/µA·cm^{-2}	v/mm·a^{-1}	b_a/V·dec^{-1}	b_c/V·dec^{-1}
40	-0.780	32.60	0.902	4.15	-3.96
60	-0.786	53.26	1.238	4.05	-3.75
80	-0.860	73.83	1.716	3.86	-3.55

In 0.4 V vs. SCE, a sharp drop in current is found in solution at 80 °C, which can be called "double anodic bottom phenomenon". This phenomenon may be related to further oxidation of corrosion product Fe$_3$O$_4$, as follows:

$2Fe_3O_4 + H_2O \rightarrow 3Fe_2O_3 + 2H^+ + 2e$ (20)
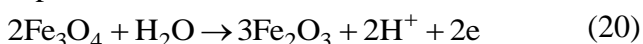
E_{pass} decreases with the increase in temperature, indicating the occurrence of passivity is easier at relative high temperature. In addition, i_{pass} increases and E_{tran} decreases sharply resulting in unstable passivity at relative high temperature.

3.2.2 EIS tests

EIS tests were conducted to study the effects of temperature on the double layer and charge transfer as well as to verify the potentiodynamic polarization curves. The tests were performed at different temperatures in the OCP. The capacitive, relatively overlapped Nyquist spectrum is shown in Fig. 4. It can be seen that the interactions are mainly governed by adsorption.
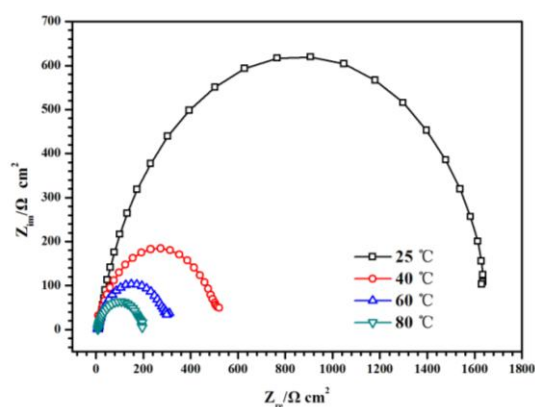
Figure 4. Nyquist plots of X80HD pipeline steels in 0.5 M $NaHCO_3$ aerated solutions at different temperatures of 25, 40, 60 and 80 ℃

Table 3. Electrochemical Impedance Spectroscopy (EIS) component values of different temperatures

$t/°C$	$R_s/\Omega\cdot cm^2$	Q_{dl}		$R_{ct}/\Omega\cdot cm^2$
		Y_0 ($W^{-1}\cdot cm^{-2}\cdot S^n$)	n_{dl}	
25	13.42	0.0001126	0.887	1617
40	9.011	0.0001688	0.8187	531.5
60	7.231	0.0002640	0.7928	301.3
80	6.028	0.0007187	0.736	140.4

The EIS results are fitted with equivalent circuit R (QR), denoting the solution resistance R_s, constant phase element (CPE) at the double layer Q_{dl}, and the charge transfer resistance R_{ct}. The CPE

reflects the non-ideal capacitance ($n<1$), as: $Z_{CPE} = [Q(jw)^n]^{-1}$, where $j = \sqrt{-1}$, and w is the angular speed. The values of electrochemical equivalent circuit elements are given in Table 3. Q_{dl} increases and R_{ct} considerably decreases with the increase in temperature. Thus, the charge transfer becomes easier with the increase in temperature, which is in accordance with the results of potentiodynamic polarization curves.

3.2.3 Corrosion morphology

The corrosion morphologies after potentiodynamic polarization tests at different temperatures are shown in Fig. 5. Cracks, approximately 10 and 40 μm, are formed at 25 and 40 °C, and no corrosion pits are observed. However, corrosion pits (30 and 50 μm diameter) are formed at 60 and 80 °C.

Energy-dispersive spectra of positions 1 and 2 show that they are rich in Al and Si respectively, indicating that they are Al-rich and Si-rich inclusions. The same results are obtained for the other cracks. Thus, these inclusions can generate cracks, indicating that the content of Al and Si should be controlled to ensure pipeline safety. In previous studies, it has also showed that the localized corrosion can be generated because of the different corrosion behavior between the inclusions and the matrix [42-44].
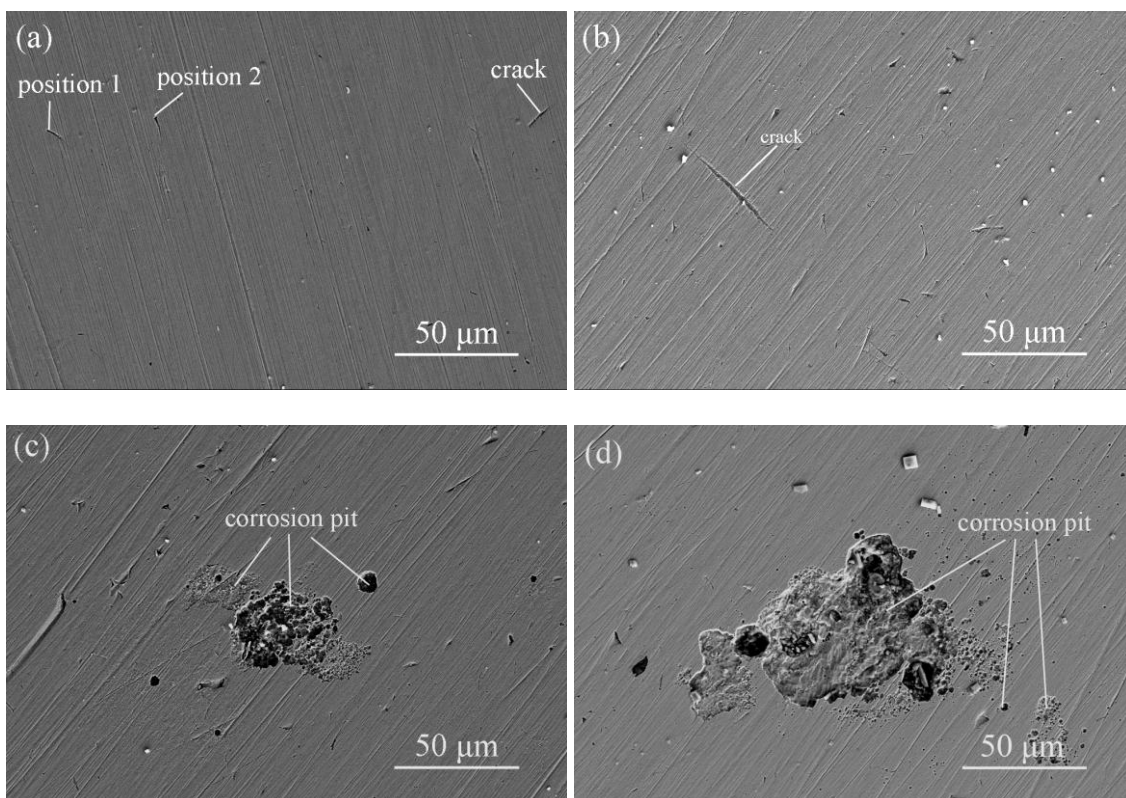

Figure 5. Corrosion morphologies of X80HD pipeline steels after potentiodynamic potential tests at different temperatures of (a) 25, (b) 40, (c) 60 and (d) 80 °C
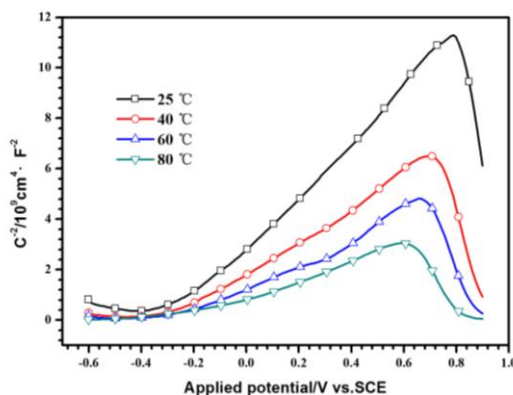
3.2.4 Potentiostatic polarization tests

The potentiostatic polarization tests were performed at 0.5 V vs. SCE at 25, 40, 60, and 80 °C under varying current densities in relation to the dissolution and polarization for 3600 s (Fig. 6). For comparison, the time was extended for 50, 100, and 150 s at 40, 60, and 80 °C. To identify the main characteristics, the values obtained for the first 100 s of potentiostatic polarization curves were discarded. The key values are shown in Table 4.

At the four temperatures, the current densities are initially scores of $\mu A \cdot cm^{-2}$, which are equal to the current densities when the potential is 0.5 V vs. SCE in potentiodynamic polarization curves. These values decrease sharply to several $\mu A \cdot cm^{-2}$, even a fraction of $\mu A \cdot cm^{-2}$, thereby indicating that the passivity can be performed from 25 °C to 80 °C. These observations are in accordance with the results of potentiodynamic polarization experiments. The current densities increase obviously with the increase in temperature from the 0 s to 3600 s.
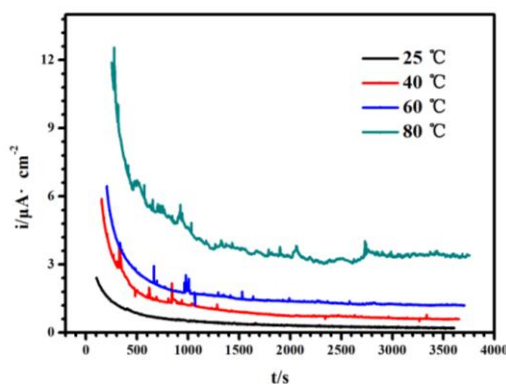
Figure 6. Potentiostatic polarization curves at 0.5 V vs. SCE of X80HD pipeline steel in 0.5 M NaHCO$_3$ solution at different temperatures for 3600 s

Figure 7. Mott-Schottky curves of X80HD pipeline steel in 0.5 M NaHCO$_3$ solution at different temperatures after potentiostatic polarized at 0.5 V vs. SCE for 3600 s

At 25 °C, no considerable fluctuations are found and the current density gradually reduces, representing stable passivity. At 40 and 60 °C, the current densities are obviously fluctuant and unstable until approximately 1500 s. The current density fluctuates all of the time at 80 °C. The

fluctuations represent the formation, ruptures, and repairs of the passive film. The stability of the passive film degrades as the temperature increases.

Table 4. The key current density values in potentiostatic polarization curves ($\mu A \cdot cm^{-2}$)

T \ t/s	6	100	500	1000	2000	3000	3600
25 °C	32.5	2.40	0.87	0.50	0.33	0.22	0.20
40 °C	63.7	6.03	1.70	1.24	0.62	0.62	0.59
60 °C	70.6	6.52	2.30	1.68	1.23	1.23	1.20
80 °C	87.7	12.1	5.50	3.98	3.41	3.41	3.39

3.2.5 Mott–Schottky analysis

The Mott–Schottky plots obtained at various pre-passivating temperatures are shown in Fig. 7. The slopes are all positive indicating that the passive films formed are n-type semiconductors, this is in accordance with previous studies [45].

The average donor density, which can be obtained using Formula (1) as a function of the temperature, is shown in Fig. 8. The average donor densities are in the order of 10^{21} cm^{-3}, indicating highly doped semiconductor structure of the passive film [33]. The average donor density increases with the increase in applied potential in the passive range and there are two straight lines (0.3 V vs.SCE is the division), demonstrating that an oxidation of Fe_3O_4 to Fe_2O_3, thereby decreasing the density. In addition, the donor density increases sharply as the temperature increases, demonstrating the degrading stability of the passive films.
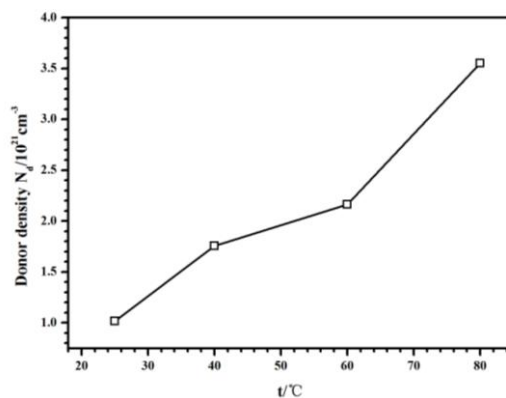
Figure 8. Effects of temperatures (25, 40, 60 and 80 °C) on donor density N_d of X80HD pipeline steel in 0.5 M NaHCO$_3$ solution after potentiostatic polarized at 0.5 V vs. SCE for 3600 s

3.2.6 Discussion on the effects of temperature

Results of the potentiodynamic polarization, electrochemical impedance spectroscopy, potentiostatic anodic polarization, and Mott–Schottky analysis indicated that the corrosion rate increases and the passivity stability weakens, with the increase in temperature. The anodic and cathodic reactions are accelerated by the increase of temperature resulting in higher corrosion rates and lower corrosion potentials [4, 8]. The similar conclusions are obtained in other solutions [46-48].

With increasing temperature, the corrosion products are easier to produce and adhered to the steel surface [49]. In addition, relatively high temperature can hinder some ions form deteriorating the passive films. Thus, the occurrence of passivity is easier at relative high temperature because of the relatively low E_{pass}. However, the E_{tran} decreases indicating low quality of the passive film in relatively high temperature [4].

The semi-conductive properties of passive film are independent on the temperature (n-type) because of the same corrosion products of iron oxide [50]. The division in 0.3 V vs.SCE can attributed to the inhomogeneous donor distribution in the passive film [51], the change in the potential of Helmholtz layer due to surface states [52] or two donor levels existing in the band gap [53]. However, the donor densities of the passive film decrease with increasing the temperature which can be attributed to the active ion exchange between matrix and solutions through the passive film. The results of Mott-schottky analysis is in accordance with the change regulars of the E_{tran} and i_{pass}. Of course, the photo-electrochemical investigations should be carried out to investigate the reasons in the near future.

4. CONCLUSIONS

The effects of atmosphere, solution concentration, and temperature on the corrosion resistance of X80HD pipeline steel in $NaHCO_3$ solution were studied by electrochemical experiments. Based on the obtained results, the following conclusions are obtained:

1. At 25 °C, passivity can be performed in $NaHCO_3$ solutions, and the presence of continuous CO_2 weakens the stability of passive film. Passivity disappears in dilute solutions with continuous CO_2.

2. The main characteristics of the potentiodynamic polarization curves are mainly determined by the atmosphere. The solution concentration and temperature mainly affect the specific values.

3. The presence of O_2 and CO_2 contributes to the corrosion of X80HD. The influence of CO_2 is relatively more significant.

4. At 25 and 40 °C, cracks can be generated from Si-rich and Al-rich inclusions. At 60 and 80 °C, corrosion pits are formed.

5. With the increase in temperature, the current densities of potentiostatic polarization increase as well as the level of fluctuations.

6. The passive film formed is an n-type semiconductor. With the increase in temperature, the donor density of passive film increases and the stability of passivity weakens.

References

1. M. Alizadeh, S. Bordbar, *Corros. Sci.*, 70 (2013) 170-179.
2. W. Zhao, Y. Zou, K. Matsuda, Z. Zou, *Corros. Sci.*, 102 (2016) 455-468.
3. Y.Z. Jia, J.Q. Wang, E.H. Han, W. Ke, *J. Mater. Sci. Technol.*, 27 (2011) 1039-1046.
4. F.F. Eliyan, A. Alfantazi, *Mater. Chem. Phys.*, 140 (2013) 508-515.
5. Z. Liu, X. Li, Y. Zhang, C. Du, G. Zhai, *Acta Metall. Sin.*, 22 (2009) 58-64.
6. W.C. Zhu, W.H. Leng, J.Q. Zhang, C.N. Cao, *Acta Metall. Sin.*, 19 (2006) 91-97.
7. P. Wang, Z. Lv, S. Zheng, Y. Qi, J. Wang, Y. Zheng, *Int. J. Hydrogen Energ.*, 40 (2015) 1-8.
8. F.F. Eliyan, E.S. Mahdi, A. Alfantazi, *Corros. Sci.,* 58 (2012) 181-191.
9. P. Bai, H. Zhao, S. Zheng, C. Chen, *Corros. Sci.*, 93 (2015) 109-119.
10. P. Liang, X. Li, C. Du, X. Chen, *Mater. Design,* 30 (2009) 1712-1717.
11. M. Zhu, C. Du, X. Li, Z. Liu, S. Wang, J. Li, D. Zhang, *Electrochim. Acta*, 117 (2014) 351-359.
12. F. Mohammadi, F.F. Eliyan, A. Alfantazi, *Corros. Sci.,* 63 (2012) 323-333.
13. H.B. Xue, Y.F. Cheng, *Electrochim. Acta*, 55 (2010) 5670-5676.
14. P. Liang, C. Du, X. Li, X. Chen, Z. liang, *Int. J. Min. Met. Mat.*, 16 (2009) 407-413.
15. W. Zhao, R. Xin, Z. He, Y. Wang, *Corros. Sci.*, 63 (2012) 387-392.
16. Y. Xu, Y. Huang, X. Wang, X. Lin, *Sensor. Actuat. B- Chem.*, 224 (2016) 37-47.
17. B. He, C.H. Lu, P.J. Han, X.H. Bai, *Eng. Fail. Anal.*, 59 (2016) 410-418.
18. D. Kong, Y. Wu, D. Long, *J. Iron Steel Res. Int.*, 20 (2013) 40-46.
19. Q. Sha, D. Li, *Mat. Sci. Eng. A- Struct.*, 585 (2013) 214-221.
20. F.M. AlAbbas, C. Williamson, S.M. Bhola, J.R. Spear, D.L. Olson, B. Mishra, A.E. Kakpovbia, *Int. Biodeter. Biodegr.*, 78 (2013) 34-42.
21. H.B. Xue, Y.F. Cheng, *Corros. Sci.*, 53 (2011) 1201-1208.
22. L.W. Wang, X.G. Li, C.W. Du, P. Zhang, Y.Z. Huang, *J. Iron Steel Res. Int.*, 22 (2015) 135-144.
23. C.I. Ossai, B. Boswell, I. Davies, *Eng. Fail. Anal.*, 60 (2016) 209-228.
24. F. Shi, L. Zhang, J. Yang, M. Lu, J. Ding, H. Li, *Corros. Sci.*, 102 (2016) 103-113.
25. X. Shi, W. Yan, W. Wang, Y. Shan, K. Yang, *Mater. Design,* 92 (2016) 300-305.
26. Y. Wang, W. Zhao, H. Ai, X. Zhou, T. Zhang, *Corros. Sci.*, 53 (2011) 2761-2766.
27. M. Yu, W. Chen, R. Kania, G. Van Boven, J. Been, *Int. J. Fatigue* 82, Part 3 (2016) 658-666.
28. O.O. Ige, L.E. Umoru, *Tribol. Int.*, 94 (2016) 155-164.
29. F.F. Eliyan, A. Alfantazi, *Corros. Sci.*, 74 (2013) 297-307.
30. I.M. Gadala, A. Alfantazi, *Corros. Sci.*, 82 (2014) 45-57.
31. B.R. Linter, G.T. Burstein, *Corros. Sci.*, 41 (1999) 117-139.
32. Y. Zhang, X. Pang, S. Qu, X. Li, K. Gao, *Int. J. Greenhouse Gas Control*, 5(2011) 1643-1650.
33. G.A. Zhang, Y.F. Cheng, *Electrochim. Acta,* 55 (2009) 316-324.
34. F.F. Eliyan, A. Alfantazi, *Corros. Sci.*, 74 (2013) 297-307.
35. L. Niu, Y.F. Cheng, *Appl. Surf. Sci.*, 253 (2007) 8626-8631.
36. M. Javidi, S. Bahalaou Horeh, *Corros. Sci.*, 80 (2014) 213-220.
37. L.Y. Xu, Y.F. Cheng, *Corros. Sci.*, 59 (2012) 103-109.
38. I.M. Gadala, A. Alfantazi, *Corros. Sci.*, 82 (2014) 45-57.
39. A.Q. Fu, X. Tang, Y.F. Cheng, *Corros. Sci.*, 51 (2009) 186-190.
40. J. Han, J. Zhang, J.W. Carey, *Int. J. Greenhouse Gas Control* 5(2011) 1680-1683.
41. G.A. Zhang, N. Yu, L.Y. Yang, X.P. Guo, *Corros. Sci.,* 86 (2014) 202-212.

42. F. Huang, J. Liu, Z.J. Deng, J.H. Cheng, Z.H. Lu, X.G. Li, *Mat. Sci. Eng. A- Struct.*, 527 (2010) 6997-7001.
43. T.Y. Jin, Y.F. Cheng, *Corros. Sci.*, 53 (2011) 850-853.
44. Z.Y. Liu, X.G. Li, C.W. Du, L. Lu, Y.R. Zhang, Y.F. Cheng, *Corros. Sci.,* 51 (2009) 895-900.
45. V.A. Alves, C.M.A. Brett, *Electrochim. Acta,* 47 (2002) 2081-2091.
46. C. Zhou, X. Chen, Z. Wang, S. Zheng, X. Li, L. Zhang, *Corros. Sci.*, 89 (2014) 30-37.
47. G. Jiang, J. Keller, P.L. Bond, *Water Res.*, 65 (2014) 157-169.
48. P. Bai, S. Zheng, C. Chen, *Mater. Chem. Phys.,* 149–150 (2015) 295-301.
49. M. Honarvar Nazari, S.R. Allahkaram, M.B. Kermani, *Mater. Design,* 31 (2010) 3559-3563.
50. D.G. Li, Y.R. Feng, Z.Q. Bai, J.W. Zhu, M.S. Zheng, *Electrochim. Acta,* 52 (2007) 7877-7884.
51. J. Shoonman, K. Vos, G. Blasse, *J. Electrochem. Soc.*, 128 (1981) 1154.
52. M.H. Dean, U. Stimming, *J. Electroanal. Chem.*, 228 (1987) 135.
53. H.H. Ge, G.D. Zhou, W.Q.Wu, *Appl. Surf. Sci.*, 211 (2003) 321-334.